Comparison of fusion cross sections for the $^{10}B + ^{16}O$ and $^{12}C + ^{14}N$ systems

J. Gomez del Campo, J. A. Biggerstaff, R. A. Dayras,* D. Shapira, A. H. Snell, P. H. Stelson, and R. G. Stokstad†
Oak Ridge National Laboratory, Oak Ridge, Tennessee 37830
(Received 2 September 1983)

The fusion cross sections for the $^{10}B + ^{16}O$ and $^{12}C + ^{14}N$ systems are compared for bombarding energies up to 18 MeV/nucleon. The energy spectra, angular distributions, and relative yields of the evaporation residues are analyzed in terms of simple kinematic considerations and Hauser-Feshbach calculations. Simultaneous determinations of mass, charge, and energy and two particle coincidence measurements at $E_{^{14}N} = 13$ MeV/nucleon support the identification of evaporation residues based on inclusive measurements of Z and E alone. The gross characteristics of the residues are consistent with the main process being complete fusion followed by equilibrium decay. The excitation functions of the $^{10}B + ^{16}O$ and $^{12}C + ^{14}N$ systems show significant differences which cannot be explained in terms of simple macroscopic models. At the highest bombarding energies the fusion cross sections decrease as $1/E_{c.m.}$ for both systems and are consistent with a maximum angular momentum limit of $\sim 27\hbar$.

I. INTRODUCTION

Measurements of fusion cross sections (σ_{fusion}) for light heavy-ion systems ($A_T + A_p \lesssim 40$) are of interest because they offer an opportunity for studying the effects of individual nucleons on the fusion process. Such effects have been reported for several p-shell and s-d shell projectile-target combinations for energies far below the fusion barrier.[1] At energies slightly above the barrier, some measurements have indicated the importance of individual nucleons (or clusters) in the fusion process, generating small oscillations in the excitation functions[2,3] or varying the maximum fusion cross sections.[4] These effects are not reproduced by current macroscopic models,[5-8] which work very well for heavier systems.

In addition, for the light systems, the isolation of the factors that limit the magnitude of the fusion cross section is of current interest. Specifically, the question is whether the limitations arise from the entrance channel or are associated with the yrast line in the compound nucleus.[9] Another subject in the study of fusion cross sections concerns absolute angular momentum limitations such as those predicted by the rotating liquid-drop model.[10]

To address the above considerations, it is desirable to have experimental data for different entrance channels that populate the same compound nucleus and for bombarding energies well in excess of the interaction barrier. We describe here the measurement of fusion cross sections for the compound nucleus ^{26}Al, produced in the reactions of $^{10}B + ^{16}O$ and $^{12}C + ^{14}N$ for bombarding energies up to 18 MeV/nucleon. Portions of these results have appeared previously in Letter publications[11-13] or in conference proceedings.[14,15] A description of the methods whereby fusion cross sections are deduced from measurements of Z and E distributions is given in Ref. 16.

After a brief description of the experimental methods (Sec. II), we review the techniques for identifying evaporation residues when their masses are comparable to or less than those of the target or projectile (Sec. III). Sections IV and V discuss the results of the time-of-flight and coincidence experiments, respectively. The sum of the direct and fusion cross sections is compared with the total reaction cross section in Sec. VI, and Sec. VII contains a discussion of incomplete fusion and preequilibrium processes. The features of the fusion excitation functions for both systems are presented and discussed in Sec. VIII.

II. EXPERIMENTAL METHODS

The experimental methods used in this study consisted of the following: (i) measurements of Z and E using ΔE-E telescopes[16]; (ii) measurements of Z, A, and E using a time-of-flight spectrometer; and (iii) two-particle coincidence experiments with pairs of ΔE-E telescopes. The majority of the experimental data was obtained using method (i). In this case, absolute cross sections were obtained through measurement of the yield, integrated beam current, detector geometry, and target thickness. Target thicknesses were measured by weighing foils of known area and by measurement of the energy loss of alpha particles. In one case, a ^{10}B beam and an ^{16}O gaseous target[17] were used. The target thickness and absolute cross sections in this case were obtained by normalization to the elastic scattering from a known admixture (0.2%) of xenon to the oxygen gas. Beams of ^{14}N at 158 and 248 MeV were provided by the Lawrence Berkeley Laboratory 88-inch cyclotron. All other beams of ^{16}O, ^{14}N, and ^{10}B were obtained from the Oak Ridge Isochronous Cyclotron. In both cases, beams were focused onto the target without the use of collimating slits; this procedure was important for obtaining clean spectra for reaction products with the same charge as the projectile.

The simultaneous measurement of mass, charge, and energy was done with the time-of-flight spectrometer at ORNL. Channel plates and thin carbon foils mounted at 45° to the 100-cm-long flight path determined the time-of-flight with a resolution of 600 psec. The energies of the particles and their atomic numbers were measured with a ΔE (ionization chamber), E (surface barrier) detector telescope. The system was able to resolve adjacent masses and atomic numbers for all reaction products through mass 22. Absolute cross sections were determined by normalization to previous measurements of Z and E made in a scattering chamber with a more accurate Faraday cup.

The coincidence measurements employed four ΔE (ionization chamber), E (surface barrier) telescopes in the experimental arrangement shown in Fig. 1. The telescope T_1 was placed at a fixed angle of 7.8° on one side of the beam. Coincidences were recorded between this counter and movable telescopes T_2–T_4 at laboratory angles from 7° to 64° on the other side of the beam. In-plane angular correlations were measured for all $Z \geq 2$ with this arrangement.

Methods (ii) and (iii) were used for the $^{14}N+^{12}C$ reaction at $E_{^{14}N} \simeq 182$ MeV. The purpose of these measurements was to check the reliability of cross sections for fusion based on measurements of Z and E distributions.

III. CHARACTERISTICS AND IDENTIFICATION OF EVAPORATION RESIDUES

For heavy-ion systems where the evaporation residue is heavier than either the target or the projectile, the determination of the mass or nuclear charge is usually enough to identify the evaporation residues. However, for systems such as $^{14}N+^{12}C$, this is not always the case, therefore one must use the additional information contained in the energy spectra. Figure 2 displays the energy spectra of fragments from neon to lithium produced in the $^{14}N+^{12}C$ reaction at $E_{^{14}N}=248$ MeV. For $Z \geq 5$, the lower energy groups with centroids of ~ 5 MeV/nucleon can be associated tentatively with the evaporation residues, since they have mean velocities characteristic of the velocity of the compound nucleus. The higher energy groups with centroids of about 18 MeV/nucleon, which are particularly prominent for $Z=6$, have velocities characteristic of the projectile, and hence they can be associated with products of direct reactions. The dashed lines shown in Figs. 2 and 3 indicate the way in which the two components were unfolded in the previous analyses. A more detailed analysis is required, however, in order to determine whether these lower energy components are consistent with the evaporation residues of a fully equilibrated compound nuclei.

A. Kinematic analysis

A description of a simple kinematic analysis of the recoil imparted to an evaporation residue was given in Ref. 16. There it was shown under certain assumptions that

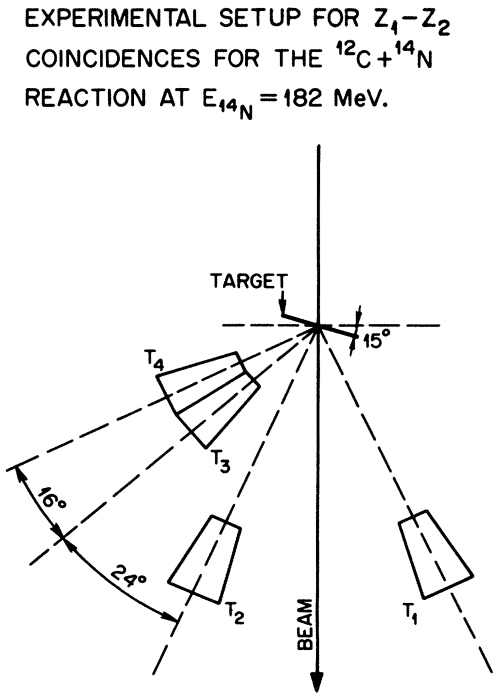

FIG. 1. Experimental setup for the coincidence measurements for the $^{14}N+^{12}C$ at $E_{^{14}N}=182$ MeV. The in-plane angular correlations for the various elements were measured by fixing the counter telescope T_1 at $\theta_{lab}=7.8°$ and varying the angles of the telescopes T_2, T_3, and T_4 in the range from 1° to 64°.

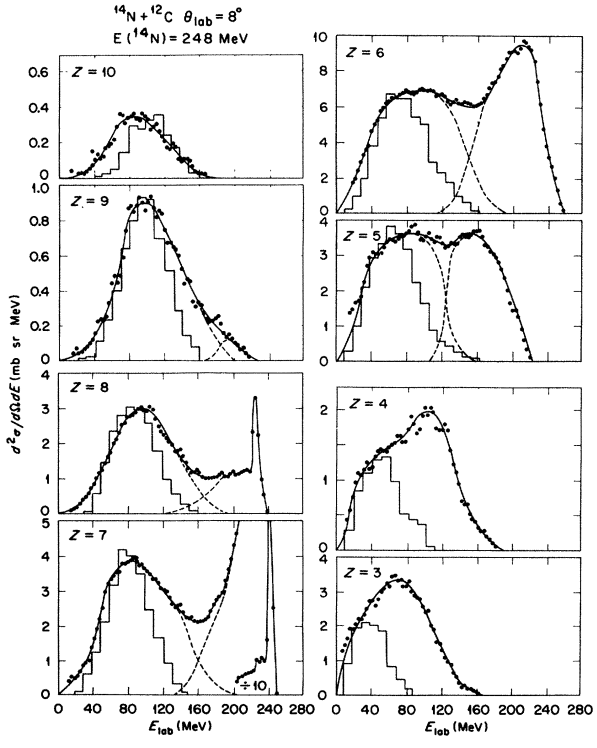

FIG. 2. Energy spectra (dots) for reaction products from $Z=10$ to 3, resulting from the collision of 248 MeV ^{14}N on ^{12}C. The dashed lines indicate the unfolding of low (ER) and high (Direct Reactions) energy components. The histograms show the results of the Monte-Carlo code LILITA.

$$\frac{1}{V_R^2}\frac{d^2\sigma}{dV_R d\Omega_L} \propto \exp[-(V_R - V_{CN}\cos\theta_L)^2/2s^2] \times \exp(-V_{CN}^2\sin^2\theta_L/2s^2) . \quad (1)$$

Here, V_R is the laboratory velocity of an evaporation residue observed at laboratory angle θ_L. The velocity of the center of mass, V_{CN}, assuming full momentum transfer, is given by

$$(A_p + A_T)V_{CN} = A_p V_p ,$$

where V_p and A_p are the velocity and mass of the projectile, and A_T is the mass of the target. The width of the Gaussian distribution at a given laboratory angle is denoted by s.

Provided that the center-of-mass velocity exceeds the maximum total recoil velocity from light particle emission, that several particles are evaporated isotropically, and that the angle of observation is not too close to 0°, the invariant velocity spectrum

$$1/V_R^2 d^2\sigma/dV_R d\Omega_L$$

should be a Gaussian with its centroid at $V_{CN}\cos\theta_L$. The conditions under which Eq. (1) is valid are discussed in more detail elsewhere.[18]

Expression (1) is compared with the experimental data in Figs. 4 and 5. Velocity spectra were determined from the energy spectra for each element by assuming a distribution of isotopes given by a Hauser-Feshbach calculation.[19] Figure 4 shows several of the invariant velocity spectra observed at $\theta_L = 8°$ for the reactions $^{12}C + ^{14}N$ at $E_{^{14}N} = 248$ MeV and $^{10}B + ^{16}O$ at $E_{^{16}O} = 168$ MeV. The solid lines are Gaussian fits to the low velocity portion of each spectrum. The dashed lines denote the portions of the spectra containing significant peripheral reaction components that were excluded from the fit. The vertical lines in Fig. 4 correspond to the predicted centroid $V_C\cos\theta_L$, and are seen to reproduce the experimental centroids quite well.

A summary of this analysis is given in Fig. 5, where the experimental centroids $\bar{V}_R$, divided by $V_{CN}\cos\theta_L$, are plotted versus the velocity of the compound nucleus V_{CN}. The solid dots correspond to the experimental centroids for the $^{14}N + ^{12}C$ system for ^{14}N bombarding energies from 86 to 248 MeV, and the open dots refer to those of the $^{10}B + ^{16}O$ system for ^{16}O bombarding energies from 93 to 203 MeV. As can be seen from Fig. 5, the ratio

$$\bar{V}_R/V_{CN}\cos\theta_L \simeq 1.0 ,$$

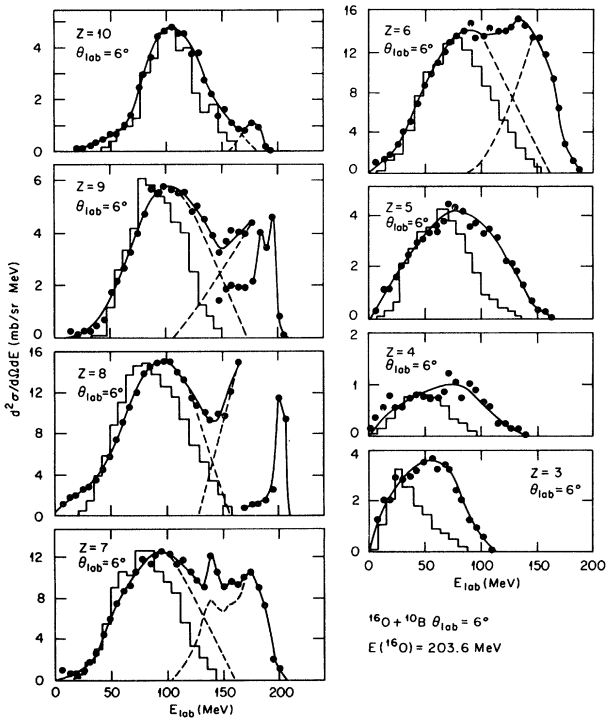

FIG. 3. Energy spectra (dots) for reaction products from $Z = 10$ to 3, resulting from the collision of 203.6 MeV ^{16}O on ^{10}B. The curves have the same meaning as in Fig. 2.

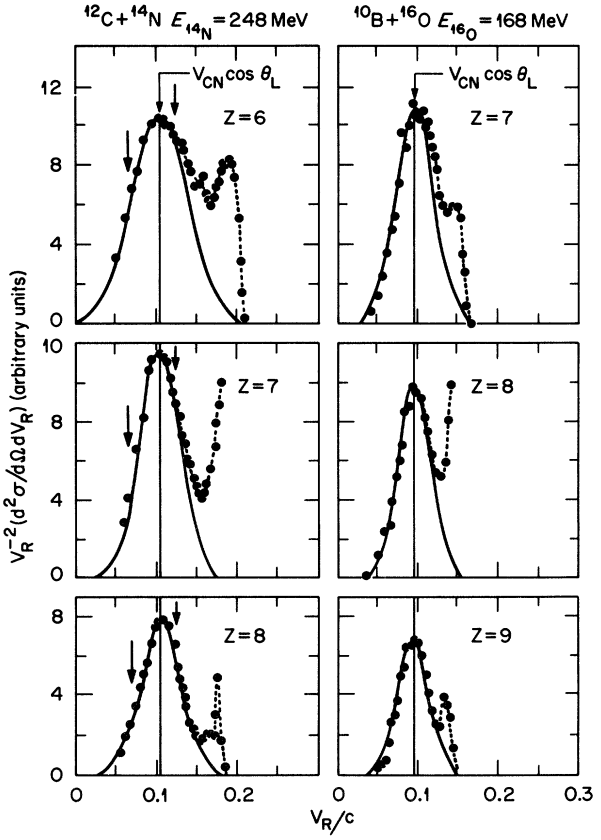

FIG. 4. Velocity distributions $V_R^{-2}d^2\sigma/d\Omega dV_R$ for reaction products of the $^{14}N + ^{12}C$ systems (left) and $^{16}O + ^{10}B$ (right) at a laboratory angle of 8°. The solid lines through the data points show the result of a Gaussian fit to the evaporation residue distributions and the vertical lines are the prediction for the centroids ($\bar{V}_R = V_{CN}\cos\theta_L$) under the assumption of full momentum transfer and equilibrium emission. The dashed lines are used to delineate the peripheral components. The vertical arrows shown for the velocity distribution of the $^{14}N + ^{12}C$ system indicate the expected centroids for fragments arising from incomplete fusion, assuming a loss of one α particle from the ^{14}N projectile.

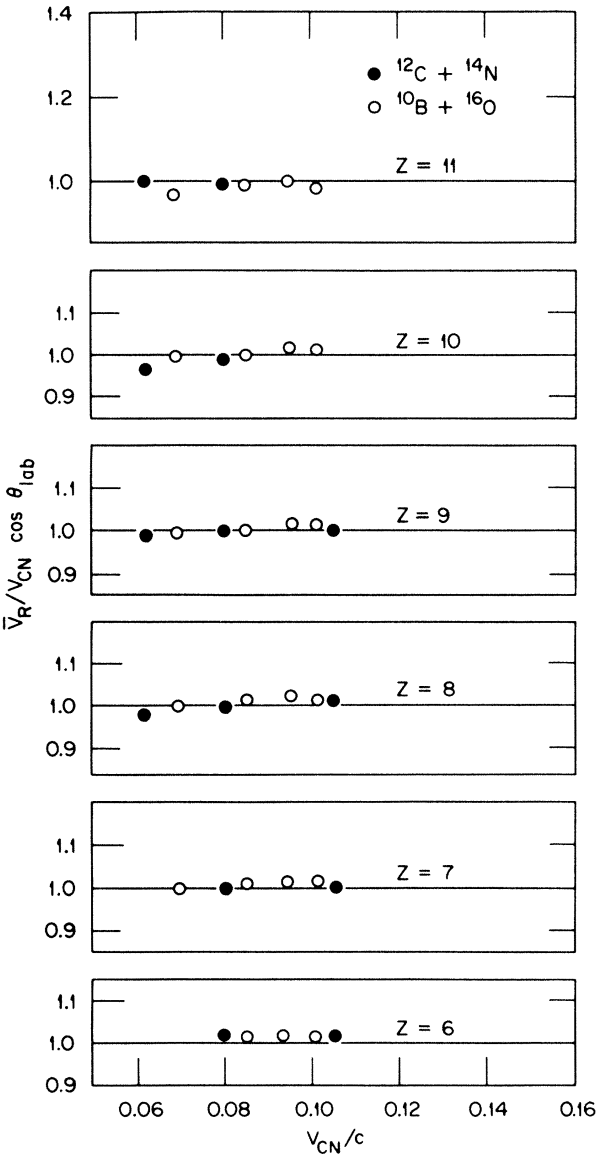

FIG. 5. Summary of the kinematical analysis for the evaporation residues of the $^{14}N+^{12}C$ (solid points) and $^{10}B+^{16}O$ (open points) systems. The vertical scale shows the centroids of the velocity distributions $\bar{V}_R$ (averaged over several laboratory angles) divided by $V_{CN}\cos\theta_L$. The horizontal scale gives the compound nucleus velocity in units of the speed of light. The lowest velocity data point corresponds to $E_{^{14}N}=86$ MeV and the highest to $E_{^{14}N}=248$ MeV.

and is independent of V_{CN} for both systems. This, again, is consistent with full momentum transfer and equilibrium decay.

B. Hauser-Feshbach Monte-Carlo calculations

The characteristics of the reaction products can also be compared to statistical model calculations to determine whether these products are consistent with the decay of a fully equilibrated compound nucleus. The Monte-Carlo code LILITA (Refs. 16 and 19) was developed in order to calculate the laboratory energy spectra and angular distributions of the evaporation residues as well as the angle-integrated yields. These calculations, described in detail in Refs. 16 and 19, are done using the Monte-Carlo method in conjunction with probability distributions derived from the Hauser-Feshbach formula.

The results of the Monte Carlo calculations are compared to the experimental data for the highest bombarding energies in Figs. 2 and 3. The calculations (histograms) are in good agreement with the portion of the oxygen and nitrogen spectra which was selected as evaporation residues. In the cases of carbon and boron, however, the calculations suggest that the empirical unfolding procedure

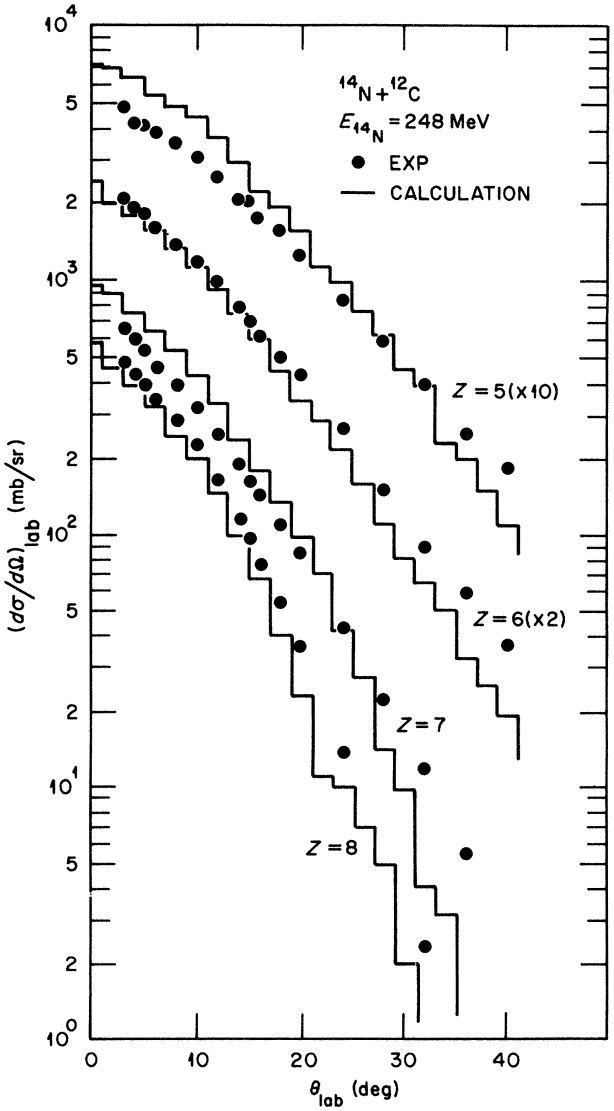

FIG. 6. Angular distributions for the evaporation residues of ^{26}Al formed by the $^{14}N+^{12}C$ entrance channel at $E_{^{14}N}=248$ MeV. The histograms show the result of the Monte-Carlo Hauser-Feshbach calculations described in the text. The experimental and theoretical angular distributions for $Z=6$ and 5 have been multiplied by the indicated factors for plotting purposes.

TABLE I. Cross sections for the $^{16}O+^{10}B$ and $^{14}N+^{12}C$.

E_{lab} (MeV)	$E_{c.m.}$ (MeV)	E_x (MeV)	σ_{fusion} (mb)	J_c h	σ_D (mb)	σ_r (mb)	σ_{om}[a] (mb)
			$^{16}O+^{10}B$				
42.0	16.15	35.68	963± 78	11.1±0.5	108±10	1071	1052
46.4	17.85	37.37	985± 78	11.9±0.5	184±18	1169	1111
50.9	19.58	39.1	985± 78	12.5±0.5	200±20	1185	1161
66.6	25.62	45.14	1160±104	15.7±0.6	160±16	1320	1271
93.5	35.96	55.48	1240±115	19.5±0.9	236±21	1476	1364
67.0[c]	41.23	60.75	1263±102	21.1±0.9	91[b]±4	1354	1393
143.2	55.09	74.6	1166±110	23.6±1.0	356±30	1522	1400
169.7	65.27	84.79	1115±100	24.0±1.0	403±40	1518	1479
203.6	78.3	97.82	955±100	25.6±1.0	454±45	1409	1579
			$^{14}N+^{12}C$				
158.0	72.92	88.06	903± 90	24.5±1.0	557±50	1460	1460
248	114.46	129.6	642± 64	26.0±1.0	809±80	1451	1515

[a]For the $^{16}O+^{10}B$ optical model calculations the optical model parameters were extracted from fits to elastic scattering at $E(^{16}O)=66.6$ and 93.4 MeV. The parameters are $r_0=1.25$, $a_0=0.52$, $r_0'=1.22$, $a_0'=0.54$, $V=28.23$, $W=0.4+0.31\,E_{c.m.}$.
[b]Direct cross sections extracted only for $Z=5$.
[c]Measurements done with an ^{16}O gas cell target and ^{10}B beam.

(dashed line) included some of the peripheral reaction component with the evaporation residues. This occurs only for these elements and at forward angles, and thus is not a major source of error. As experience in the use of these Monte Carlo statistical model calculations has increased, so has the confidence in their reliability and accuracy. Therefore, it now seems desirable to use the calculation more directly in the unfolding of the experimental data, rather than to rely solely on the shape of the experimental spectra. The data have been reanalyzed and cross sections correspondingly adjusted. The revised values are given in Table I. The maximum change in any fusion cross section has been 10%. All conclusions based on the earlier analysis are still valid.

Comparisons of the experimental angular distributions of evaporation residues with the Monte-Carlo calculations (histograms) are shown in Figs. 6 and 7. The solid data points correspond to the unfolding of the spectra, as given by the dashed lines in Figs. 2 and 3. At these bombarding energies, the evaporation residue cross sections from $Z=5$ to 8 constitute 85% of the fusion cross section. For most of the elements, the calculated angular distributions follow the trend of the experimental data for two orders of magnitude and give supporting evidence for the proper identification of the evaporation residues. (At large angles and for products with small Z, there may be contributions from low energy recoils of the direct reaction products. This has a negligible effect on the deduced fusion cross section.) For these bombarding energies the compound nucleus excitation energy is 129 MeV ($^{14}N+^{12}C$) and 98 MeV ($^{16}O+^{10}B$), corresponding to nuclear temperatures of $T\sim 6.1$ and 5.3 MeV, respectively. In spite of the high temperature, there does not appear to be any evidence of sizable preequilibrium effects (see Sec. VII).

Since the $^{14}N+^{12}C$ and $^{10}B+^{16}O$ systems populate the same compound nucleus, ^{26}Al, the assumption of equilibrium decay for these systems can be tested in a model independent way by comparing the relative yield distributions for cases where the compound nucleus is formed at the same excitation energy and angular momentum. Such a comparison is shown in Fig. 8 for the two excitation energies in ^{26}Al, $E_x=44$ MeV (top) and $E_x=97$ MeV (bottom). The relative yields are given for the $^{14}N+^{12}C$ system by the dashed histograms and those for the $^{10}B+^{16}O$ system by the solid lines. The similarities observed at both high and low excitation energies indicate that the same compound system is formed and that its decay is independent of the entrance channel. For comparison, the predictions of the statistical model are shown (as solid bars) in Fig. 8. The agreement is quite good.

IV. CHARGE AND MASS DISTRIBUTIONS

Measurements of the energy spectra for individual isotopes provide a more stringent comparison of the statistical model with experimental data and can also facilitate the separation of residues from direct reaction products. Figure 9 shows energy spectra for the isotopes of carbon, produced at $\theta_L=6°$ in the reaction $^{14}N+^{12}C$ at $E_{^{14}N}=182$ MeV. Note that the direct reaction component is completely absent from the ^{14}C spectrum. Production of ^{14}C by a direct process would require simultaneous exchange of a proton and a neutron—an unlikely process. The separation between the direct products and the evaporation residues is quite clear for ^{13}C. The Monte Carlo predictions of the evaporation residue spectra are given for each isotope by the histograms, which have been normalized to the data in each case.

A similar comparison is given in Fig. 10 for a laboratory angle of 12°. Note the much reduced direct reaction component. The angle integrated yields for each isotope of boron, carbon, nitrogen, and oxygen are shown in Fig. 11 and are compared with the statistical model prediction.

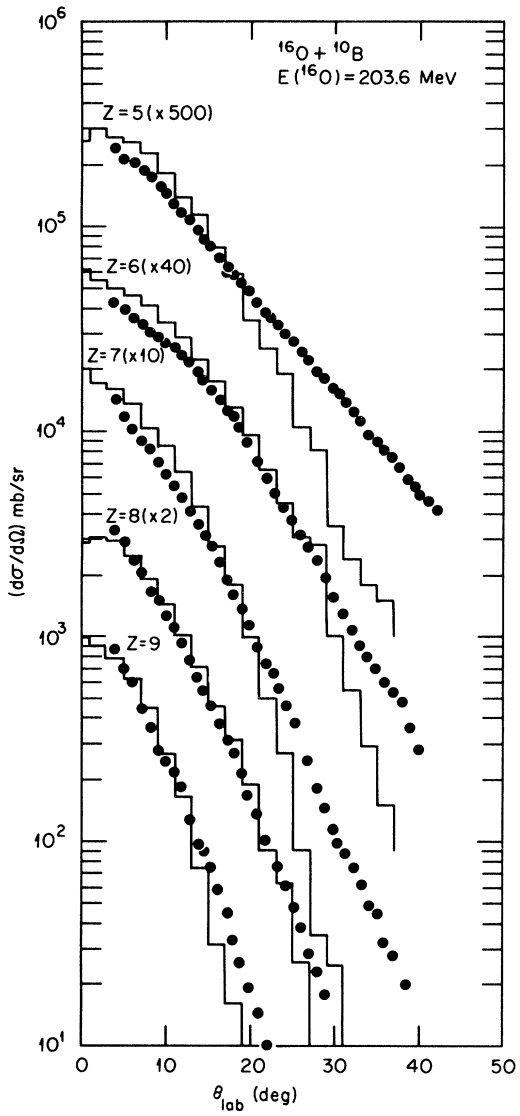

FIG. 7. Angular distributions for the evaporation residues of 203.6 MeV ^{16}O on ^{10}B. The histograms show the results of the Monte-Carlo Hauser-Feshbach calculations.

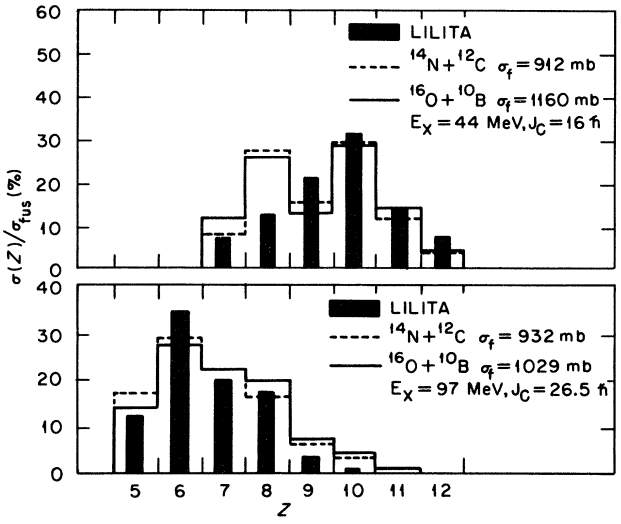

FIG. 8. Comparisons of the experimental angle integrated yields of evaporation residues for $^{16}O + ^{10}B$ (solid histogram) and $^{14}N + ^{12}C$ (dashed histogram) at low and high excitation energies. σ_f is the measured fusion cross section and J_c is the deduced critical angular momentum.

The only discrepancy of note concerns ^{12}C and ^{11}B. The predicted amounts of ^{11}B and ^{12}C depend critically upon the treatment of proton emission just above the threshold. Since the predicted yield of ^{12}C is too high by the same amount that the ^{11}B is too low, we expect that this does not represent a serious discrepancy with the evaporation code and could be removed by a reasonable adjustment of the parameters affecting the proton decay of ^{12}C.

V. COINCIDENCE MEASUREMENTS

More direct information on the nature of the reaction mechanism can be obtained from coincidence measurements. An evaporation residue should have associated with it only those light particles, e.g., protons, neutrons, and α particles, which were evaporated. Direct reactions, on the other hand, should produce two bodies with masses near those of the target and projectile, each of which might have an excitation energy sufficient to evaporate a few mass units after emerging from the primary collision region. A direct reaction product thus should appear in coincidence with another fragment of comparable mass. This could be a particle with a charge, e.g., of 5, 6, 7, or 8. This can be tested by observing heavy-ion, heavy-ion coincidences with the apparatus shown in Fig. 1. The spectra of carbon ions detected at 8° in coincidence with ions of boron, carbon, and nitrogen are shown in Fig. 12(b). The coincidence yield has been integrated over all (in-plane) angles of the recoil particles. Note the similarity of this coincidence spectrum with the portion of the singles spectrum in Fig. 12(a) which is labeled as the direct component. In particular, the evaporation residues are not in coincidence with another fragment of charge 5 or higher. The evaporation residues are in coincidence with α particles, however, as is shown in Fig. 12(c). Alpha particles are also associated with direct reaction products, since the primary reaction products can be excited above the threshold for α-particle emission. It is clear that the α-particle multiplicity is larger for evaporation residues than for direct reaction products.

The above comparison of the coincidence results with qualitative expectations for the characteristics of evaporation residues and direct reaction products indicates that the separation of these two mechanisms, based on the singles measurements alone, is reasonable. A more stringent test, however, is the angular correlation of α particles in coincidence with the residues. Figure 13 shows a comparison of such data with the statistical model prediction (histogram). Subsequent experiments have enabled a more extensive, quantitative comparison of the α-particle multiplicities, energy spectra, and angular distributions in coincidence with the residues.[20] These results and the Monte Carlo statistical model calculations also compare favorably.

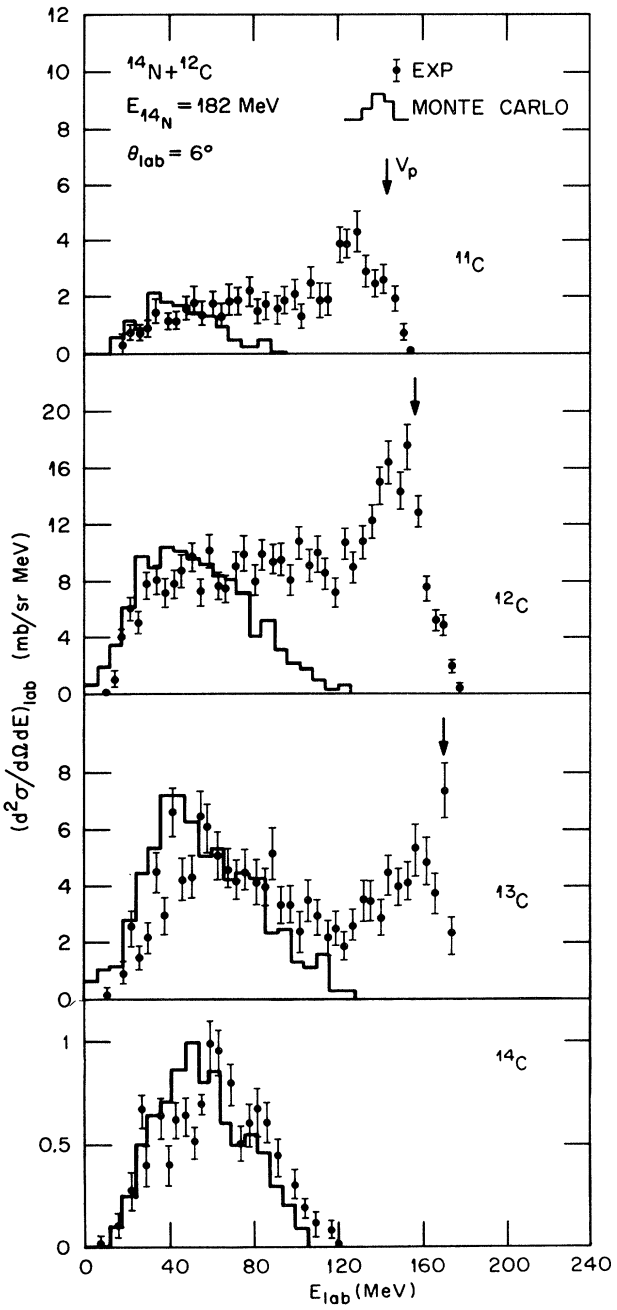

FIG. 9. Energy spectrum (dots) for carbon isotopes measured at $\theta_{lab}=6°$ by the time-of-flight technique for the reaction 182 MeV $^{14}N+^{12}C$. The histograms show the prediction of the code LILITA.

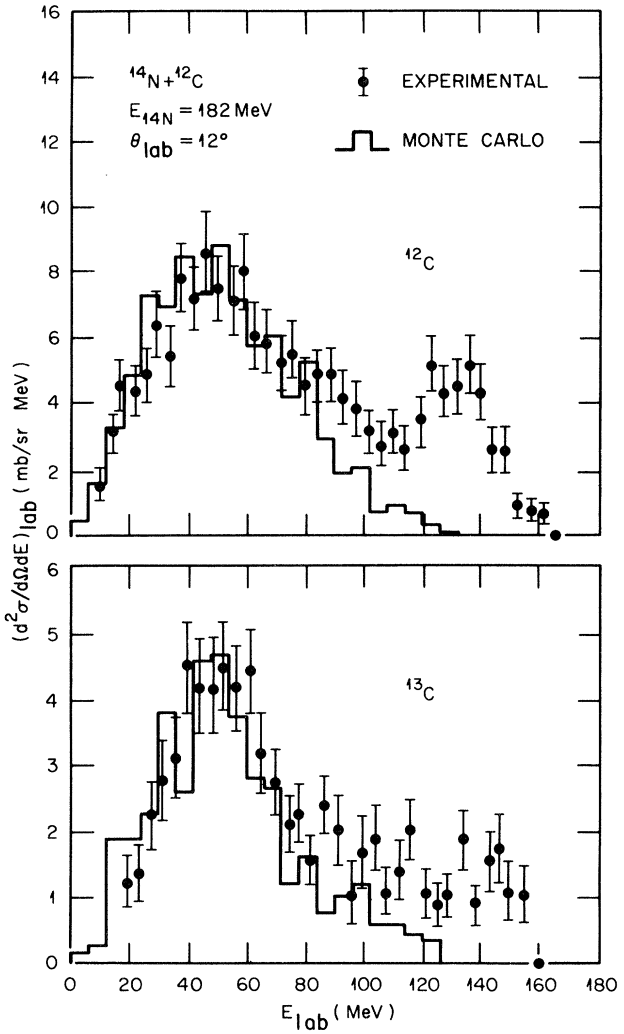

FIG. 10. Energy spectrum (dots) and statistical model calculations for carbon isotopes measured at $\theta_{lab}=12°$.

VI. TOTAL REACTION CROSS SECTION

The double-peaked shape of the energy spectra observed at forward angles (Figs. 2 and 3) has led naturally to the classification of the reaction products. The sum of these two cross sections should give the total reaction cross section, provided no products have been lost (e.g., through detection thresholds) and there has been no double counting of fragments. The total reaction cross section was obtained independently through an optical model analysis of the elastic scattering (see Ref. 16). The energy dependence of σ_R was determined by an analysis at several energies and by a comparison with a series of extensive measurements made on a similar system, $^{12}C+^{12}C$.[21,22]

A comparison of σ_R obtained by adding σ_{fusion} and σ_{direct} with σ_R (optical model) is made in Fig. 14. The system $^{10}B+^{16}O$ is included in this comparison. Note the good agreement and, in particular, the relatively smooth behavior of σ_R in the high energy region. This is important in that it shows that reaction products are not escaping detection.

VII. INCOMPLETE FUSION AND PREEQUILIBRIUM PROCESSES

The most extensive comparisons of the experimental data with the statistical model have been made for the reaction $^{14}N+^{12}C$ at $E_{^{14}N}=13$ MeV/nucleon. The results of this comparison do not indicate major discrepancies be-

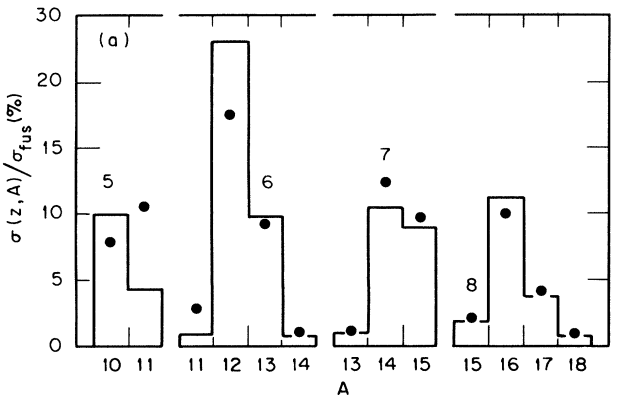

FIG. 11. Relative yield of evaporation residues measured by the time-of-flight technique for the reaction 182 MeV $^{14}N+^{12}C$. The histograms show the Monte Carlo calculation.

tween the expectations for complete fusion followed by equilibrium decay and the observed characteristics of the evaporation residues. It is on this basis that cross sections for fusion have been deduced. It is possible, of course, that nonequilibrium processes are present to some extent at 13 MeV/nucleon and that they result in reaction products having characteristics sufficiently similar to evaporation residues that it becomes difficult to identify them. We also expect that the intensity of any nonequilibrium processes will increase with increasing bombarding energy. Since our definition of fusion is an operational one, reaction products whose characteristics agree with the statistical model predictions will be classified as such. It thus becomes a question of how accurately one can predict these characteristics and how extensive and complete are the experiments to which they will be compared.

There have been a number of measurements in the last few years in which beam (and higher) velocity α particles have been detected in coincidence with heavy residues.[23–26] In cases involving rare earth targets, characteristic gamma rays show that the remainder of the projectile was captured by the target. This type of reaction is referred to as incomplete fusion or massive transfer. In other cases,[27,28] it also appears likely that a significant (but not full) amount of momentum was transferred to the target. One must inquire to what extent such processes might be present in the $^{14}N+^{12}C$ and $^{10}B+^{16}O$ reactions, especially for reactions at bombarding energies above 10 MeV/nucleon.[29]

Incomplete fusion implies incomplete momentum transfer and, therefore, a different velocity of the compound system. In our experiment, the average velocities of the residues all agree with the expectation for full momentum transfer (see Figs. 4 and 5), even for the highest bombarding energies. The vertical arrows in Fig. 4 denote the centroids expected for fragments arising from an incomplete fusion reaction assuming that an alpha particle in the ^{14}N projectile is a "spectator" and continues with the beam velocity while the remaining ^{10}B is captured. This results in a compound system having a lower velocity. It is also possible that an alpha particle in the

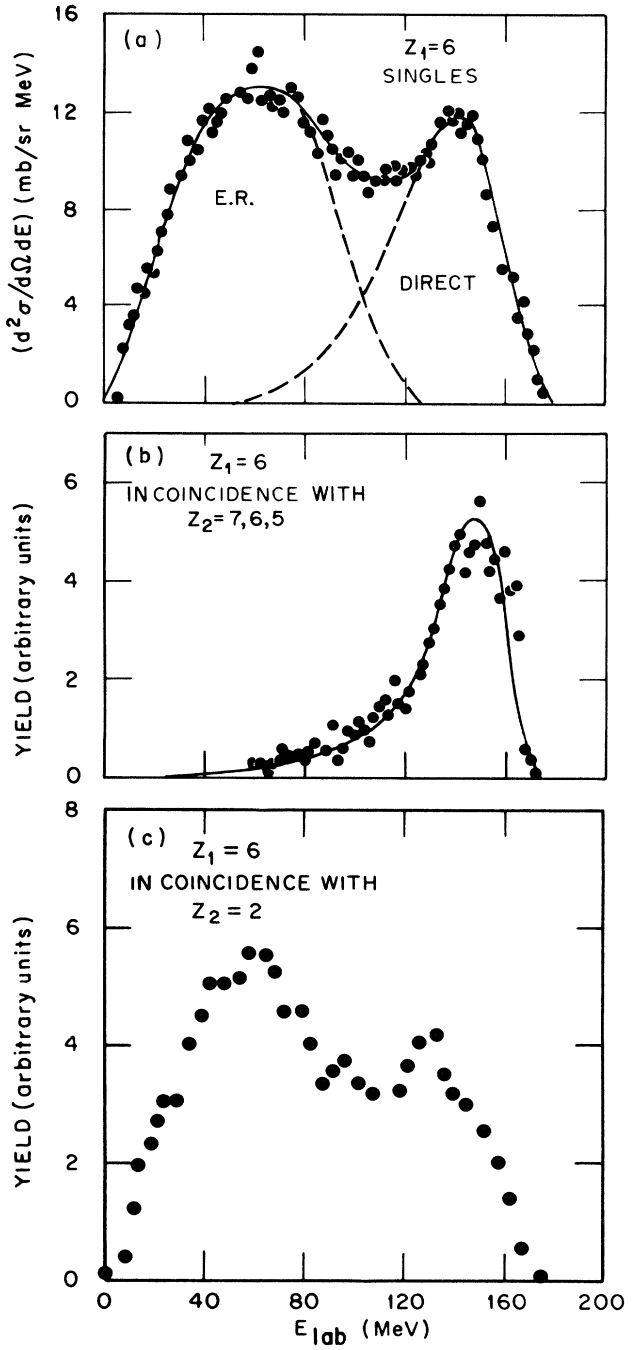

FIG. 12. Energy spectrum of carbon ions at $\theta_{lab}=7.8°$ for $E(^{14}N)=182$ MeV. (a) Singles spectrum displaying the evaporation residue and direct reaction components. (b) Spectrum for $Z_1=6$ after integration of the coincidence angular correlation for associated fragments of nitrogen, carbon, and boron. (c) Spectrum for $Z_1=6$ after integration of coincidence, the angular correlation for associated α particles.

^{12}C target is a spectator and receives no transferred momentum. In this case, the ^{14}N projectile effectively fuses with a ^{8}Be target and produces a compound system with a higher velocity. Inspection of Fig. 4 indicates that there is no major component of either of these processes

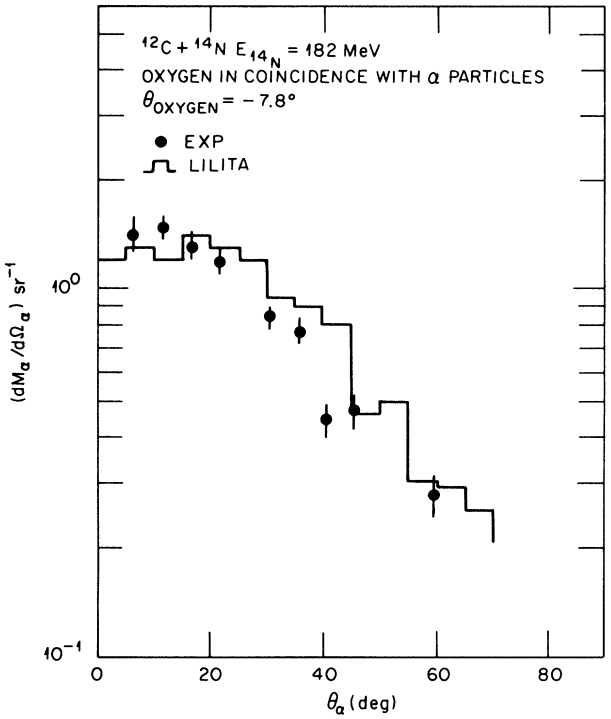

FIG. 13. The angular correlation of α particles in coincidence with evaporation residues having $Z=8$.

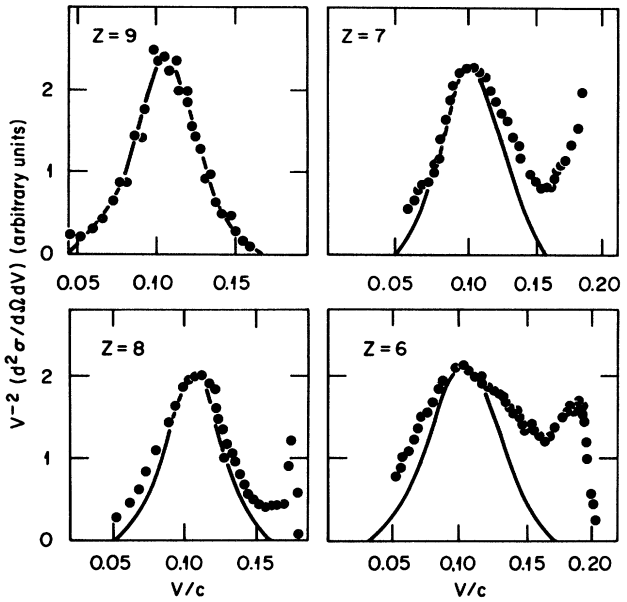

FIG. 15. Velocity spectra of fluorine, oxygen, nitrogen, and carbon fragments for the $^{14}N+^{12}C$ reaction at E (^{14}N)=248 MeV and at $\theta_{lab}=8°$. The solid curves are the results of complete fusion calculations using the Monte-Carlo code LILITA.

present. However, the presence of both such incomplete fusion components in nearly equal proportions would leave the location of the centroid approximately unchanged. In fact, for identical projectile and target nuclei, the centroid would be exactly the same as incomplete fusion, and the only effect would be a symmetric broadening of the velocity spectrum. Calculations of the velocity distributions for the complete fusion of 248-MeV $^{14}N+^{12}C$ are shown in Fig. 15 (solid curves) and, as can be seen, the predicted widths are generally smaller than the widths of the evaporation residue portion of the yield (lower energy groups for $Z \leq 8$), an effect that can be accounted for by the incomplete fusion mechanism. At 182 MeV (Fig. 10) this effect is much smaller. It is difficult to place upper limits on the amounts of incomplete fusion present by an examination of the width of the distribution (especially if one considers a single nucleon as a spectator). Nevertheless, Monte-Carlo calculations have been used for the two extreme cases of 248-MeV $^{14}N+^{8}Be$ and $(\frac{10}{14})\times 248$ MeV $^{10}B+^{12}C$. The results of these calculations (arbitrarily normalized to the data) are shown in Fig. 16, where the solid histograms correspond to $Z=8$ evaporation residues coming from the $^{10}B+^{12}C$ fusion, and the dotted one to those of the fusion of $^{14}N+^{8}Be$. These comparisons indicate that neither of the above processes alone can account for the data; however, a combination of both plus complete fusion can. From a fit to the energy spectrum shown in Fig. 16, we conclude that incomplete fusion in the form of $^{10}B+^{12}C$ capture and $^{14}N+^{8}Be$ capture could be present in the amounts of 10% and 15%, respectively, in the $Z=8$ spectrum at $\theta_{lab}=8°$.

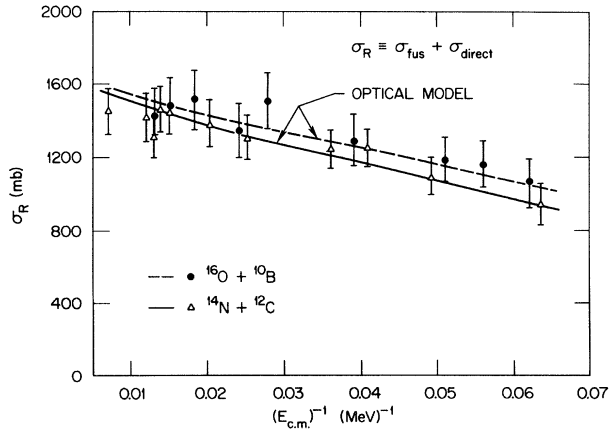

FIG. 14. The total reaction cross section for $^{10}B+^{16}O$ and $^{12}C+^{14}N$ obtained by adding the measured direct and compound components. The values obtained from optical model parameters are based on fits to elastic scattering.

VIII. DISCUSSION

Attempts to understand the behavior of fusion cross sections in light systems fall generally into two extreme categories—those which emphasize either the properties of the projectile and target, i.e., the entrance channel, or those based on the properties of the compound nucleus. However, the time evolution from entrance channel to compound nucleus is continuous and the properties of the intermediate stages must also be important. While there

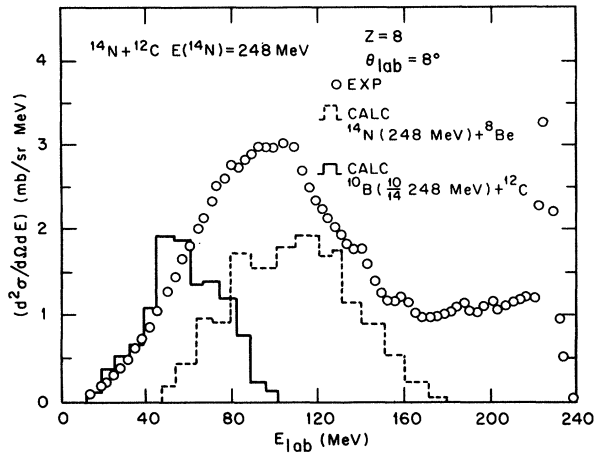

FIG. 16. Energy spectra of oxygen fragments for the $^{14}N+^{12}C$ reaction at E (^{14}N)=248 MeV and at $\theta_{lab}=8°$. The dotted and dashed histograms are the results of incomplete fusion Monte-Carlo calculations discussed in the text.

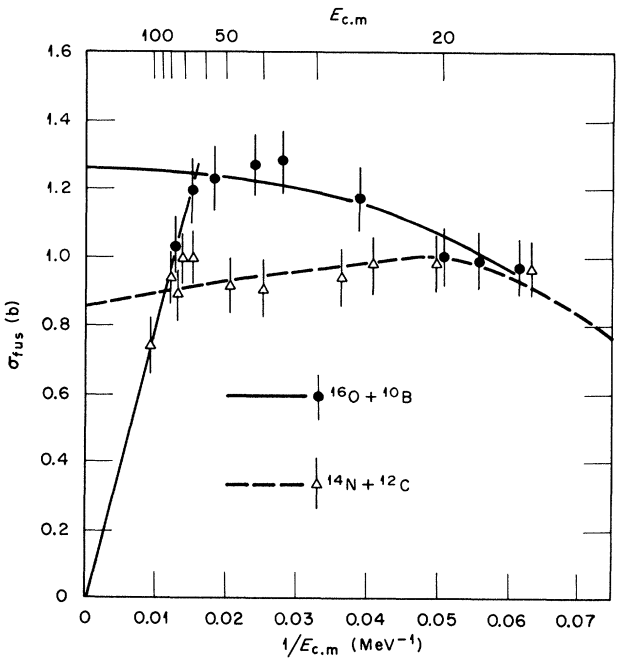

FIG. 17. Fusion cross sections plotted against $(E_{c.m.})^{-1}$ for $^{10}B+^{16}O$ and $^{12}C+^{14}N$. The solid and dashed curves show fits to the data using the parametrization of Glas and Mosel. The straight line passing through the origin gives the expected trend of σ_{fusion} for a constant maximum angular momentum of $27\hbar$.

are theoretical treatments which consider the intermediate stages—the two center shell model[30] and the time-dependent Hartree-Fock approximation[31] are examples—the consideration of the two extremes is useful and it may provide important clues to the reaction mechanism.

The discussion of fusion reactions usually centers around limitations on the fusion cross section or limitations on the critical angular momentum for fusion. Both the entrance channel and the compound nucleus place limits on fusion. At energies near the Coulomb barrier there are many compound nuclear states available and the barrier in the entrance channel is the limiting factor. At very high energies the entrance channel may bring in an angular momentum larger than the compound nucleus can support. In this case, the compound nucleus does not exist and therefore is not formed. At intermediate energies there must be a transition from the one form of limit to the other. The questions are the following: (i) Which mechanism imposes the more restrictive limit? (ii) What is the element of nuclear structure that is responsible for the limit?

A. Entrance channel models

The experimental fusion cross sections are shown in Fig. 17 and are plotted versus $(E_{c.m.})^{-1}$. The curved solid and dashed lines in Fig. 17 are fits to the data using the Glas and Mosel parametrization.[7] The parameters are ($^{12}C+^{14}N$, $^{10}B+^{16}O$) r_B (fm)=(1.4, 1.5); $V(R_B)$ (MeV) =(6.7,6.7);r_{cr}=(1.11, 1.35); $V(R_{cr})$=(−1.9, 2.5); $\hbar\omega$ (MeV)=(2,2). Note the large difference in the reduced parameters describing the location of, and the potential at, the inner critical radius. They reflect the large differences for these two systems already apparent in Fig. 17. Such large variations in the cross sections are not explained by an $A^{1/3}$ variation in the nuclear radii.

Birkelund *et al.*[6] have studied the systematics of fusion cross sections in the context of an entrance channel model by solving the classical equations of motion for a real proximity potential and a proximity one-body frictional force. Without an *ad hoc* adjustment of parameters, they obtain reasonably good agreement for the $^{12}C+^{14}N$ fusion cross section. The prediction for $^{10}B+^{16}O$ is very similar to that for $^{12}C+^{14}N$ and therefore does not reproduce the data. This is not surprising, since the global approach of their analysis excludes the variation of parameters to fit each case.

Nuclear radii do not vary exactly as $A^{1/3}$, however, and the effects of this on the fusion cross section can be estimated. Folding model calculations,[32] which incorporate mean-square radii determined by electron scattering, indicate that $^{12}C+^{14}N$ and $^{10}B+^{16}O$ have the same mass overlap at radii of 1.11 and 1.15 times $(A_1^{1/3}+A_2^{1/3})$, respectively. Incorporating this in the Glas and Mosel formulation produces a maximum predicted difference in the cross section of 7%. While in the right direction, this accounts for only about one-fifth of the observed difference. Vandenbosch[8] has calculated fusion cross sections with a classical trajectory model incorporating the proximity potential and one-body friction (similar to Birkelund *et al.*[6]), but has used radii and diffuseness parameters taken from electron scattering results. These calculations predict differences between $^{10}B+^{16}O$ and $^{12}C+^{14}N$ which are from one-third to one-half of the observed differences. However, the overall energy dependence is not well reproduced, especially at low energies.

From the above, we may conclude (for $^{12}C+^{14}N$ and $^{10}B+^{16}O$) that either the entrance channel is not the most important limiting factor for fusion in the region of

$E_{c.m.} \sim 20$—70 MeV, or, if the entrance channel is not the important factor, then individual nucleons may be playing a critical role in a way not described by macroscopic calculations.

B. Compound nucleus models

The properties of the compound nucleus are its excitation energy, $E_x = E_{c.m.} + Q$, and the maximum angular momentum at which it is formed, J, given by $(J+1)^2 = \sigma_{fusion}/\pi\lambda\!\!\!^{-2}$. Figure 18 shows E_x vs $J(J+1)$ for the compound nucleus ^{26}Al. If, for example, the compound nucleus were the limiting factor on σ_{fusion} at all energies and for entrance channels, then all the data points in Fig. 18 should determine a single locus. This is clearly not the case. At low excitation energies, differences are expected because the Coulomb barrier (or outer interaction barrier) is the important factor. At high energies, the liquid drop limit[10] should set in, and this is apparent for the highest energies in Fig. 18.

It is clear that, in the intermediate energy region, the limiting angular momenta for $^{12}C+^{14}N$ and $^{10}B+^{16}O$ determine separate loci. Thus, strictly speaking, the compound nucleus cannot be the limiting factor for *both* $^{12}C+^{14}N$ and $^{10}B+^{16}O$. It is true that the differences between $^{10}B+^{16}O$ and $^{12}C+^{14}N$ shown in Fig. 18 appear smaller when the data are plotted as E_x vs $J(J+1)$. A contributing factor to this is the $\sim$4-MeV difference in Q values for the two reactions. The square-root dependence of J or σ_{fusion} also makes the differences appear smaller. The Saclay group[33] has examined a number of different reactions leading to the same compound nucleus and finds, in general, that the differences in Q value are in the direction such that a plot of E_x vs J^2 produces loci closer to each other than when the data are plotted as σ_{fusion} vs $E_{c.m.}$. This trend has been noted in another form, viz., the variation of σ^{max} from system to system, by Lee *et al.*[34] However, no Q value shift can eliminate the crossing (or different slopes) of the loci shown in Fig. 18.

If it were possible to know independently the location of the yrast line, then it would be obvious whether the entrance channel or the compound nucleus is the limiting factor. An indication of its location can be obtained from theoretical calculations. Glas and Mosel[9] and Diebel *et al.*[35] have used the Strutinsky method for rotating nuclei to calculate yrast lines in the mass region from $A=24$ to 60. Their results for $A=26$ are indicated in Fig. 18 and suggest that fusion reactions do not populate, and therefore are not limited by, the yrast line of a rapidly rotating, highly deformed, but otherwise "cold" nucleus. The nu-

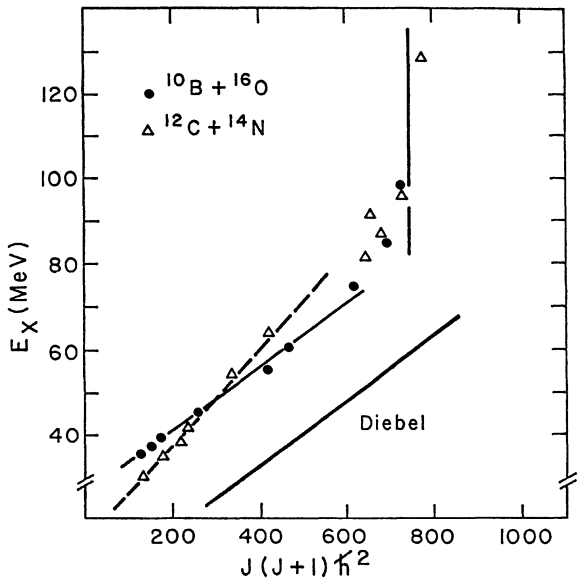

FIG. 18. Plot of the excitation energy vs J^2 for the $^{10}B+^{16}O$ and $^{12}C+^{14}N$ systems. Note the different slopes of the loci for $J^2 < (25)^2\hbar^2$. The curve labeled "Diebel" is the calculated yrast line given in Ref. 35.

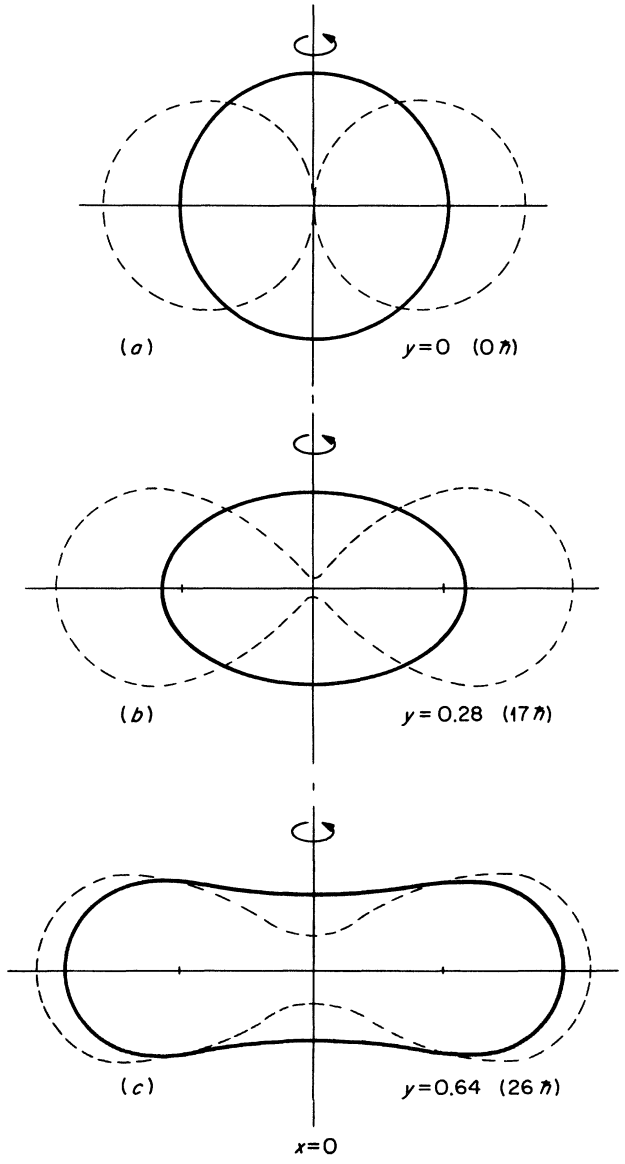

FIG. 19. The shapes of a nucleus with $A \sim 26$ as predicted by the rotating liquid drop model (see Ref. 10). The dashed curves show the saddle point configuration, and the solid ones, those of the ground state.

clear system produced in a high energy collision will have some thermal excitation and therefore be displaced from the cold yrast line. It appears reasonable that the structure of the cold yrast line is carried over to an effective yrast line relevant for fusion. This approach has been followed by Lee *et al.*[34] who assume that the effective yrast line lies parallel to the cold yrast line. A fit to a number of data suggests that the shift is ~ 10 MeV if the cold yrast line is calculated with a rigid body moment of inertia having a radius parameter $r_0 = 1.2$ fm. However, there are significant deviations between experiment and this parametrization, and the measured slopes of σ_{fusion} are not always reproduced.[36]

Another method of defining an effective yrast line has been proposed by Vandenbosch.[37] The argument is made that fusion will occur when the compound nucleus is far enough above the yrast line such that the average width of levels Γ divided by the average spacing is the order of unity. The value of Γ is obtained from the empirical correlation of experimental values given by Shapira *et al.*[38] and the spacing of levels from the compilation of Gilbert and Cameron.[39] (There is an uncertainty in the location of this line connected with the uncertainty in the density of levels.) The comparison with experiment is favorable, particularly for the higher J values. At lower J values, $J \lesssim 20$, the data lie further above the yrast line. As noted by the authors,[37] this suggests that the properties of the entrance channel are the more stringent limiting factor at bombarding energies just above the break in $\sigma_{\text{fusion}}(E)$. This interpretation may be contrasted with that of Lee *et al.*[34] who assume their statistical yrast limitation is valid down to energies at which $\sigma^{\max}$ is reached. Finally, a consideration of kinetic energy and angular conservation by Von Oertzen leads to the conclusion that the yrast line is not reached at moderate energies and that it is the dynamics of the entrance channel that limit fusion.[40]

At the highest bombarding energies the rotating liquid drop limit—the angular momentum for which the barrier against fission vanishes—becomes a quantity of importance. The data for $^{12}C+^{14}N$ and $^{10}B+^{16}O$ exhibit such a maximum angular momentum, and the value (see Fig. 18) is consistent with that of the rotating liquid drop model.[10] It is interesting to consider the predicted shape of the ^{26}Al nucleus at this limit. The dashed line in Fig. 19 (from Ref. 10) shows the shape of the saddle point configuration and the solid line that of the ground state configuration. At $26\hbar$ the shapes are nearly identical. (At $26.6\hbar$, they are identical.) The configuration at the liquid drop limit is very similar to that of a carbon ion and nitrogen ion in close contact. Thus, in this limit, the concepts of compound nucleus and entrance channel merge.

The similarity of the saddle point shapes (dashed lines) in Fig. 19 with the shape of the entrance channel at the point when the ions first interact also has provided a partial justification for treating the fusion process in a one-dimensional model. Heavier systems have thicker necks at the saddle point and thus require an explicit treatment of the neck degree of freedom in their formation. Nevertheless, the large differences between the fusion cross sections for $^{10}B+^{16}O$ and $^{12}C+^{14}N$ call into question the neglect of the necking degree of freedom. It is the valence nucleons that should play an important role in the formation of a neck at the onset of the fusion process; the different nuclear structures of ^{10}B, ^{12}C, ^{14}N, and ^{16}O may be influencing the fusion cross section in just this way.

The above discussion has focused on fusion and has neglected the process which competes with it for the flux making up the total reaction cross section. This process is the direct or peripheral reaction. The elements of nuclear structure (presence of collective levels, etc.) and reaction mechanism governing the strength of the direct reaction channels are of equal importance in understanding fusion cross sections. There have been a number of promising efforts in this direction.[41,42]

It seems likely that a future understanding of the fusion cross sections for light systems in the intermediate energy region will have to encompass both the entrance channel (including competition with the direct reactions) and the properties of the compound and precompound nucleus.

This research was supported by the U.S. Department of Energy under Contract No. W-7405-eng-26 with the Union Carbide Corporation.

---

*Present address: Centre d'Etudes Nucléaires de Saclay, 91191 Gif-sur-Yvette Cedex, France.

†Present address: Lawrence Berkeley Laboratory, Berkeley, California 94704.

[1]R. G. Stokstad, Z. E. Switkowski, R. A. Dayras, and R. M. Weiland, Phys. Rev. Lett. 37, 888 (1976).

[2]P. Sperr, T. H. Braid, Y. Eisen, D. G. Kovar, F. W. Prosser, Jr., J. P. Schiffer, S. L. Tabor, and S. Vigdor, Phys. Rev. Lett. 37, 321 (1976).

[3]J. J. Kolata, R. C. Fuller, R. M. Freeman, F. Haas, B. Heusch, and A. Gallman, Phys. Rev. C 16, 891 (1977).

[4]D. G. Kovar, D. F. Geesaman, T. H. Braid, Y. Eisen, W. Henning, T. R. Ophel, M. Paul, K. E. Rehn, S. J. Sanders, P. Sperr, J. P. Schiffer, S. L. Tabor, S. Vigdor, B. Zeidman, and F. W. Prosser, Jr., Phys. Rev. C 20, 1305 (1979).

[5]R. Bass, Nucl. Phys. A231, 45 (1974); Phys. Rev. Lett. 39, 265 (1977).

[6]J. R. Birkelund, J. R. Huizenga, J. N. De, and D. Sperber, Phys. Rev. Lett. 40, 1123 (1978).

[7]D. Glas and U. Mosel, Nucl. Phys. A237, 429 (1975).

[8]R. Vandenbosch, Nucl. Phys. A339, 167 (1980).

[9]D. Glas and U. Mosel, Phys. Lett. 78B, 9 (1978).

[10]S. Cohen, F. Plasil, and W. J. Swiatecki, Ann. Phys. (N.Y.) 82, 557 (1974).

[11]R. G. Stokstad, J. Gomez del Campo, J. A. Biggerstaff, A. H. Snell, and P. H. Stelson, Phys. Rev. Lett. 36, 1529 (1976).

[12]R. G. Stokstad, R. A. Dayras, J. Gomez del Campo, P. H. Stelson, C. Olmer, and M. Zisman, Phys. Lett. 70B, 289 (1977).

[13]J. Gomez del Campo, R. A. Dayras, J. A. Biggerstaff, D.

Shapira, A. H. Snell, P. H. Stelson, and R. G. Stokstad, Phys. Rev. Lett. 43, 26 (1979).
[14]J. Gomez del Campo, Notas Fis. 3, 74 (1980).
[15]R. G. Stokstad, Nukleonika 26, 373 (1981).
[16]J. Gomez del Campo, R. G. Stokstad, J. A. Biggerstaff, R. A. Dayras, A. H. Snell, and P. H. Stelson, Phys. Rev. C 19, 2170 (1979).
[17]D. Shapira, R. A. Dayras, J. L. C. Ford, Jr., J. Gomez del Campo, A. H. Snell, P. H. Stelson, and R. G. Stokstad, Nucl. Instrum. Methods 163, 325 (1979).
[18]J. Gomez del Campo *et al.* (private communication).
[19]J. Gomez del Campo and R. G. Stokstad, LILITA, a Monte Carlo Statistical Model Code, Oak Ridge National Laboratory Technical Memo No. ORNL-TM-7295, 1981 (unpublished).
[20]D. E. DiGregorio, J. Gomez del Campo, D. Shapira, D. C. Hensley, J. A. Biggerstaff, M. E. Ortiz, and Y. D. Chan (private communication).
[21]R. G. Stokstad, R. M. Weiland, G. R. Satchler, C. B. Fulmer, D. C. Hensley, S. Raman, L. A. Rickertsen, A. H. Snell, and P. H. Stelson, Phys. Rev. C 20, 655 (1979).
[22]A. J. Cole, W. D. Rae, M. E. Brandan, A. Dacal, B. G. Harvey, R. Legrain, M. J. Murphy, and R. G. Stokstad, Phys. Rev. Lett. 47, 1705 (1981).
[23]T. Inamura, M. Ishihata, T. Fukuda, T. Shimoda, and H. Hiruta, Phys. Lett. 69B, 51 (1977).
[24]K. Siwek-Wilczynska, E. H. DuMarchie Van Voorthuysen, J. Van Popta, R. H. Siemssen, and J. Wilczynski, Phys. Rev. Lett. 42, 1599 (1979).
[25]D. R. Zolnowski, H. Yamada, S. E. Cala, A. C. Kahler, and T. T. Sugihara, Phys. Rev. Lett. 41, 92 (1978).
[26]K. A. Geoffroy, J. B. Natowitz, R. C. Eggers, and M. V. Namboodiri, Nucl. Phys. A302, 310 (1978).
[27]P. Gonthier, H. Ho, M. N. Namboodiri, L. Adler, J. B. Natowitz, S. Simon, K. Hagel, R. Terry, and A. Khodai, Phys. Rev. Lett. 44, 1387 (1980).
[28]B. B. Back, K. L. Wolf, A. C. Mignerey, C. K. Gelbke, T. C. Awes, H. Breuer, V. E. Viola, Jr., and J. P. Dyer, Phys. Rev. C 22, 1927 (1980).
[29]V. E. Viola, Jr., B. B. Back, K. L. Wolf, T. C. Awes, C. K. Gelbke, and H. Breuer, Phys. Rev. C 26, 178 (1982); H. Morgenstern, W. Bohne, K. Grabish, D. G. Kovar, and H. Lehr, Phys. Lett. 113B, 463 (1982); Y. D. Chan, M. Murphy, R. G. Stokstad, I. Tserruya, S. Wald, and A. Budzanowski, Phys. Rev. C 27, 447 (1983).
[30]J. Y. Park, W. Greiner, and W. Scheid, Phys. Rev. C 21, 958 (1980).
[31]H. Flocard, S. E. Koonin, and M. S. Weiss, Phys. Rev. C 17, 1682 (1978).
[32]R. Satchler and W. G. Love, Phys. Lett. 65B, 415 (1976).
[33]J. P. Wieleczko, S. Harar, M. Conjeaud, and F. Saint-Laurent, Phys. Lett. 93B, 35 (1980).
[34]S. M. Lee, T. Matsuse, and A. Arima, Phys. Rev. Lett. 45, 165 (1980).
[35]M. Diebel, D. Glas, U. Mosel, and H. Chandra, Nucl. Phys. A333, 253 (1980).
[36]Y. D. Chan, D. E. DiGregorio, J. L. C. Ford, Jr., J. Gomez del Campo, M. E. Ortiz, and D. Shapira, Phys. Rev. C 25, 1410 (1982).
[37]R. Vandenbosch and A. J. Lazzarini, Phys. Rev. C 23, 1074 (1981); R. Vandenbosch, Phys. Lett. 87B, 183 (1979).
[38]D. Shapira, R. G. Stokstad, and D. A. Bromley, Phys. Rev. C 10, 1063 (1974).
[39]A. Gilbert and A. G. W. Cameron, Can. J. Phys. 43, 1446 (1965).
[40]W. Von Oertzen, Z. Phys. A 297, 295 (1980).
[41]D. Pelte and U. Smilansky, Phys. Rev. C 19, 2196 (1979).
[42]O. Tanimura, Phys. Lett. 90B, 50 (1980).